Supplementary Information for

Governing PbI_6 Octahedral Frameworks for High-Stability Perovskite Solar Modules

Qifan Feng,[1,#] Xiaofeng Huang,[1,#] Ziheng Tang,[1] Yaolin Hou,[1] Qing Chang,[1] Siqing Nie,[1] Fang Cao,[1] Xiaoying Niu,[1] Jun Yin,[1,2] Jing Li,[1,2] Nanfeng Zheng,[1.2] and Binghui Wu[1,2,*]

[1] Pen-Tung Sah Institute of Micro-Nano Science and Technology, Jiujiang Research Institute, State Key Laboratory for Physical Chemistry of Solid Surfaces, Collaborative Innovation Center of Chemistry for Energy Materials, National & Local Joint Engineering Research Center of Preparation Technology of Nanomaterials, College of Chemistry and Chemical Engineering, Xiamen University, Xiamen 361005, China

[2] Innovation Laboratory for Sciences and Technologies of Energy Materials of Fujian Province (IKKEM), Xiamen 361102, China

Methods

Materials. 4-Vinylaniline (VAn, 97%), bis (trifluoromethane) sulfonimide lithium salt (Li-TFSI, 99.95%), DMF (99.8%), 4-tert-butylpyridine (*t*BP, 96%), and acetonitrile (99.8%) were purchased from Sigma-Aldrich; Titanium diisopropoxide bis (2,4-pentanedionate) (75% in isopropanol), SnO_2 colloids (15 wt% in H_2O), cesium iodide (CsI), chlorobenzene (99.9%) from Alfa Aesar; zinc acetate (99%), ethanolamine (99%), *N*-Methylpyrrolidone (NMP, 99.5%), and trifluoromethanesulfonic acid (99%) from Energy Chemical; formamidinium iodide (FAI) from GreatCell Solar; lead (II) iodide (PbI_2, 99.99%) from TCI Chemicals; Methylammonium chloride, TiO_2 paste, and Spiro-OMeTAD from Xi'an Polymer Light Technology Corp. All the chemicals were used as received without further purification.

Synthesis of VT molecules. 1.192 g (10 mmol) of 4-Vinylaniline (VAn, 119.16 g/mol, stored in a freezer prior to use) was added to 10 mL of cold isopropanol (cooled in an ice-water bath). 1.073 mL (12 mmol) of a solution of 99% HSO_3CF_3 (150.07 g/mol, 1.696 g/mL) was added dropwise to the cooled VAn/isopropanol mixture. This mixture was left to react for 2 h, and then slowly warmed up to room temperature. The residual

solvent was evaporated under reduced pressure to obtain yellow powders. Then as-collected yellow powders were purified by dissolving in isopropanol and subsequently re-precipitated with diethyl ether. The purification process was repeated three times, and the products were kept under vacuum for 16 h before being stored in a nitrogen glovebox.

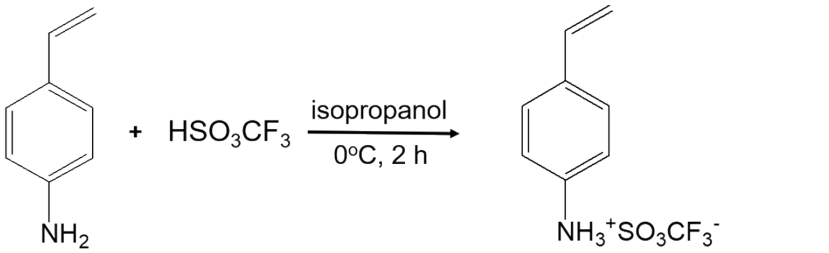

4-Vinylaniline Vinylaniline trifluoromethanesulfonate (VT)

Synthesis of VAnI molecules.1.192 g (10 mmol) of 4-Vinylaniline (VAn, 119.16 g/mol, stored in a freezer prior to use) was added to 10 mL of cold isopropanol (cooled in an ice-water bath). 1.921 mL (12 mmol) of a solution of 47% HI (127.91 g/mol, 1.7 g/mL) was added dropwise to the cooled VAn/isopropanol mixture. This mixture was left to react for 2 h, and then slowly warmed up to room temperature. The residual solvent was evaporated under reduced pressure to obtain yellow powders. Then as-collected yellow powders were purified by dissolving in isopropanol and subsequently re-precipitated with diethyl ether. The purification process was repeated three times, and the products were kept under vacuum for 16 h before being stored in a nitrogen glovebox.

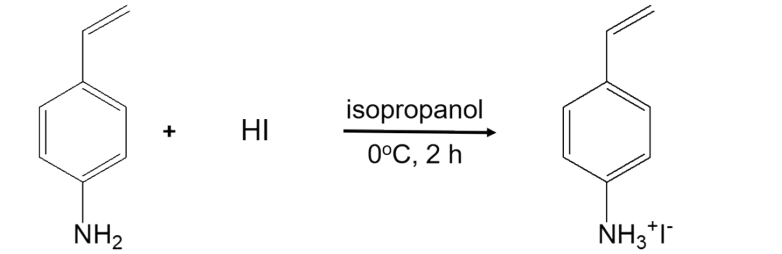

4-Vinylaniline Vinylaniline iodine (VAnI)

Fabrications of PSCs and PSMs. The FTO glass (NSG, Tec-7) was cleaned ultrasonically with detergent, deionized water, acetone, and ethanol successively. The $ZnTiO_3$-ZnS compact layer was fabricated according to our previous work.[1] For depositing of the $FACsPbI_3$ films, a solution containing CsI (0.03 mmol), FAI (0.97

mmol), PbI_2(1.00 mmol), and dimethylformamide (DMF) (600 μL) with additives (20 mg of MACl and 96 μL of NMP) was spun on the $ZnTiO_3$/FTO substrate (25 μL for 2 × 2 cm^2 and 60 μL for 6 × 6 cm^2) at 6000 rpm for 30 s. Then diethyl ether was added on the wet film at 3 s prior to the end of the spin-coating process, and the as-prepared film was annealed at 110°C for 30 min and 130°C for 30 min in N_2 atmosphere. For the PVT post-treatment, the PVT/isopropanol solution (0.01-0.25 mg/mL) was deposited on the $FACsPbI_3$ perovskite layer by spin-coating (6000 rpm, 20 s) or blade-coating, followed by UV irradiation for 5 min. Subsequently, a drop (15 μL for 2 × 2 cm^2 and 60 μL for 6 × 6 cm^2) from chlorobenzene solution (each milliliter containing 73.2 mg Spiro-OMeTAD, 8.6 μL of acetonitrile containing Li-TFSI (520 mg/mL) and 14.4 μL of *t*BP was coated via solution process at 4,000 rpm for 20 s to get the hole transport layer. For the NiPc HTL, a 60-μL drop of a trichloromethane solution (10 mg/mL nickel phthalocyanine) was deposited by spin-coating at 3000 rpm for 30 s. The evaporation of 60 nm gold electrodes to fabricate on the top of hole transport layer to complete device fabrication. The active area of 2 × 2 cm^2 and 6 × 6 cm^2 devices was defined by 0.12-cm^2 and 18-cm^2 masks, respectively.

The large-area (10 × 10 cm^2) perovskite films were prepared by blade-coating vacuum-flash technology according to our previous work.[2] A droplet of perovskite precursor (40 μL) was added into the gap (~200 μm) between the blade and substrate, and then the blade moved parallel with a speed of 16 mm/s. Next, the wet film was transferred into a vacuum chamber in a short time, which could be quickly pumped to 10 Pa from atmospheric pressure within 1 min, and then maintained for 15 s at this pressure. After the vacuum-flash process, the substrate was annealed at 110°C for 30 min and 130°C for 30 min at atmosphere. For the PVT post-treatment, the isopropanol solution of PVT (0.03 mg/mL) was also bladed with a speed of 40 mm/s under ambient condition with relative humidity ~30%, followed by UV irradiation for 5 min. The spiro-OMeTAD was deposited by blade-coating with a speed of 40 mm/s under ambient condition with relative humidity ~30%. The active area of the solar module after P1-P2-P3 laser-scribing process was calculated to be 54 cm^2.

The modules (6 × 6 cm^2 or 10 × 10 cm^2) consisted of 8 or 14 sub-cells connected in series were scribed on a laser engraving machine (P1, ZNL1810V2, Hangzhou Zhongneng Optoelectronic Technology Co., LTD., China). For fabrication of solar modules, three laser-patterning lines, P1 (200 μm), P2 (200 μm), and P3 (200 μm) were accomplished by the laser beam with a power of 18, 10 and 7 W, respectively. After P2 (200 μm) laser pattern lines were completed, the isopropanol solution of PVT (0.1 mg/mL) was deposited on the HTL layer by spin-coating (6000 rpm, 20 s) / blade-coating (40 mm/s) followed by UV irradiation for 5 min. After P3 (200 μm) laser pattern lines were completed, the isopropanol solution of PVT (1 mg/mL) was deposited on the gold electrode by spin-coating (4000 rpm, 20 s) / blade-coating (40 mm/s) followed by UV irradiation for 5 min. The schematic diagram of laser post-scribing modification (P2, P3) process was shown in Figure S19.

Heat and Damp Test. For the heat-damp test (85°C and 85% RH), NiPc with excellent moisture and heating stability was chosen as hole transport layer and PIB-based polymer sealant (polyisobutylene) was used for module encapsulation. Note that the device for heat-damp test was designed as a 4 × 4 cm^2 module (active area 10 cm^2) based on 6 × 6 cm^2 module substrate.

Device Characterizations. The Raman spectra of perovskite thin films were obtained using a high-resolution dispersive Raman microscope (LabRAM HR Evolution, Horiba) equipped with an argon ion continuous-wave laser (λ = 532 nm) at room temperature. The ESI-ToF experiment was carried out on the ultra-High performance liquid chromatography-quadrupole time-of-flight mass spectrometer (Agilent 1290-6545XT). Surface/cross-sectional morphologies and EDS mapping of the perovskite films or devices were carried out on a field-emission SEM apparatus (Sigma, ZEISS). *J*−*V* characteristics of devices were analyzed on a solar simulator (Class 3A, 94023A, Newport) under AM1.5 G standard light equipped with a Keithley 2400 source meter. IPCE spectra were measured on an IPCE system (Newport), which was calibrated with a certified Si-reference cell. X-ray photoelectron spectroscopy and ultraviolet photoelectron spectroscopy (UPS) measurement was performed on an Escalab Xi^+ Thermo Fisher instrument. The XRD patterns of perovskite films were obtained on an

X-ray diffractometer (Smart Lab-SE, Rigaku). The HS-LEISS experiment was carried out on a Qtac100 instrument with Ne^+ ion source. Trap state densities of the perovskite films have been analyzed by the SCLC model using the typical configurations (FTO/ NiO_x / $FACsPbI_3$ / P3HT/ Au). The trap densities were calculated by formula of $V_{TFL}= qN_{trap}d^2/2\varepsilon\varepsilon_0$.[2] The UV−vis spectra were recorded on a LAMBDA 1050^+. The steady and time-resolved PL spectra were measured using a PL spectroscope (HORIBA Scientific, iHR 320) excited by a 375-nm pulsed laser. Atomic force microscopy (AFM) for surface topography and potential and characteristics of perovskite films was measured on an atomic force microscope equipped with a controller using a Pt/Ir-coated Si tip.

First-principle calculations by density functional theory. The first-principle calculations were performed in the frame of density functional theory (DFT) with the program package CASTEP,[3, 4] using the plane-wave ultra-soft pseudopotential (PW-USPP) method and the Perdew-Burke-Ernzerhof (PBE) form of generalized-gradient approximation (GGA) exchange-correlation energy functional.[5] The structure optimization of $FAPbI_3$ was carried out using means of the Broyden-Fletcher-Goldfarb-Shanno (BFGS) algorithm by allowing all atomic positions to vary and relaxing lattice parameter. The isolated $CF_3SO_3^-$ ions, vinylaniline trifluoromethanesulfonate and poly(vinylaniline) trifluoromethanesulfonate molecules were put in 20 Å × 10 Å × 10 Å lattices to perform the structure optimizations. They would stop until the total energies were converged to 10^{-5} eV/atom, the forces on each unconstrained atom were smaller than 0.3 eV/Å, the stresses were lower than 0.05 GPa and the displacements were less than 0.001 Å. The plane-wave cutoff, E_{cut}, was chosen to 340 eV. The k-point mesh of 4×4×4 $Å^3$ was used for Brillouin zone (BZ) sampling of $FAPbI_3$.

Note for depth resolved GIXRD measurement

The $\sin^2\varphi$-2θ technique is a common X-ray diffraction (XRD) technique to evaluate residual strain in polycrystalline thin films.[6] According to the Bragg's Law and generalized Hooke's Law,[7] the $\sin^2\varphi$-2θ equation about stress σ and 2θ can be obtained as follow:

$$\sigma = -\frac{E}{2(1+v)}\frac{\pi}{180^o}cot\theta_0\frac{\partial(2\theta)}{\partial(sin^2\varphi)} \quad (1)$$

where E is the perovskite modulus, v is Poisson's ratio of the perovskites. E was evaluated by AFM, and v was evaluated as 0.3 according to previous work.[8] θ_0 and θ were the diffraction peak for stress free perovskite (*hkl*) crystal plane and the experimental perovskite thin films, respectively. It must be emphasized that the instrument angle (ω, ψ, θ) and diffraction geometry angles (φ) are no longer equivalent when grazing incident method is using to test strain.

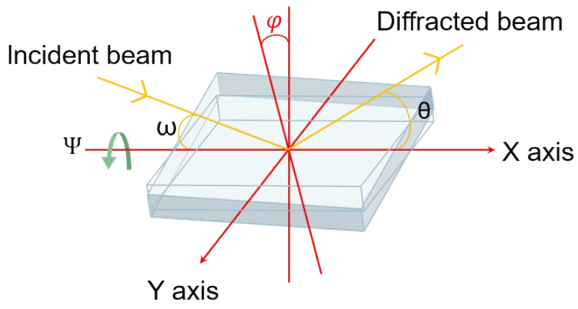

The φ is the angle of the diffraction vector with respect to the sample normal direction. To realize the continuous change of angle φ, we rotated the sample stage around the X axis (increasing the instrumental angle ψ). The relationships between the instrumental angles (ω, ψ, θ) and the diffraction geometry angles (φ) are described with the equation as follows:

$$cos\varphi = cos\psi\, cos\,(\omega - \theta) \quad (2)$$

where θ is 7.02° and ω is around 0.5°. The calculation results of residual stress are list in Table S3.

Once we define:

$$C = -\frac{E}{2(1+v)}\frac{\pi}{180^o} \quad (3)$$

$$k = \frac{\partial(2\theta)}{\partial(sin^2\varphi)} \quad (4)$$

the Equation (1) will be simplified and stress σ can be obtained as follows:

$$\sigma = Ck \quad (5)$$

When determining the diffraction angle, C is a negative constant and there is a linear function between 2θ and $\sin^2\varphi$. k is the slope of the $\sin^2\varphi$-2θ plot. According to the formula (5), by judging the slope of $\sin^2\varphi$-2θ line, the state of the residual stress σ can be obtained. When $k > 0$, the negative σ value is indicative of compressive stress. When $k < 0$, the positive σ value is indicative of tensile stress.

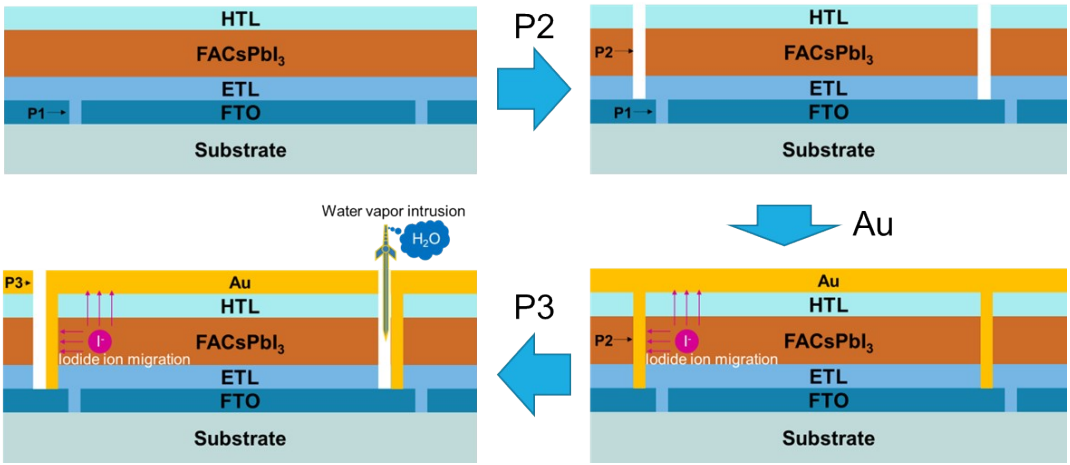

Figure S1. Schematic illustration of the laser-scribing (P2 and P3) processes for traditional PSMs. The perovskite-involved interfaces should be considered to ensure the overall stability of whole PSMs.

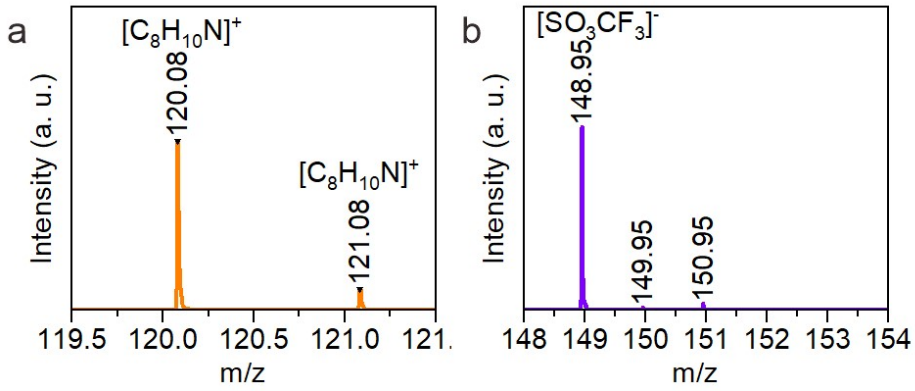

Figure S2. LC-Q-ToF-MS spectra of vinylaniline trifluoromethanesulfonate (VT) in isopropanol in the form of (a) positive ion mode and (b) negative ion mode. The appearance of $[C_8H_{10}N]^+$ and $[SO_3CF_3]^-$ fragment peaks within VT solution corresponds to vinyl aniline cations and trifluoromethanesulfonate anions in the isopropanol, respectively.

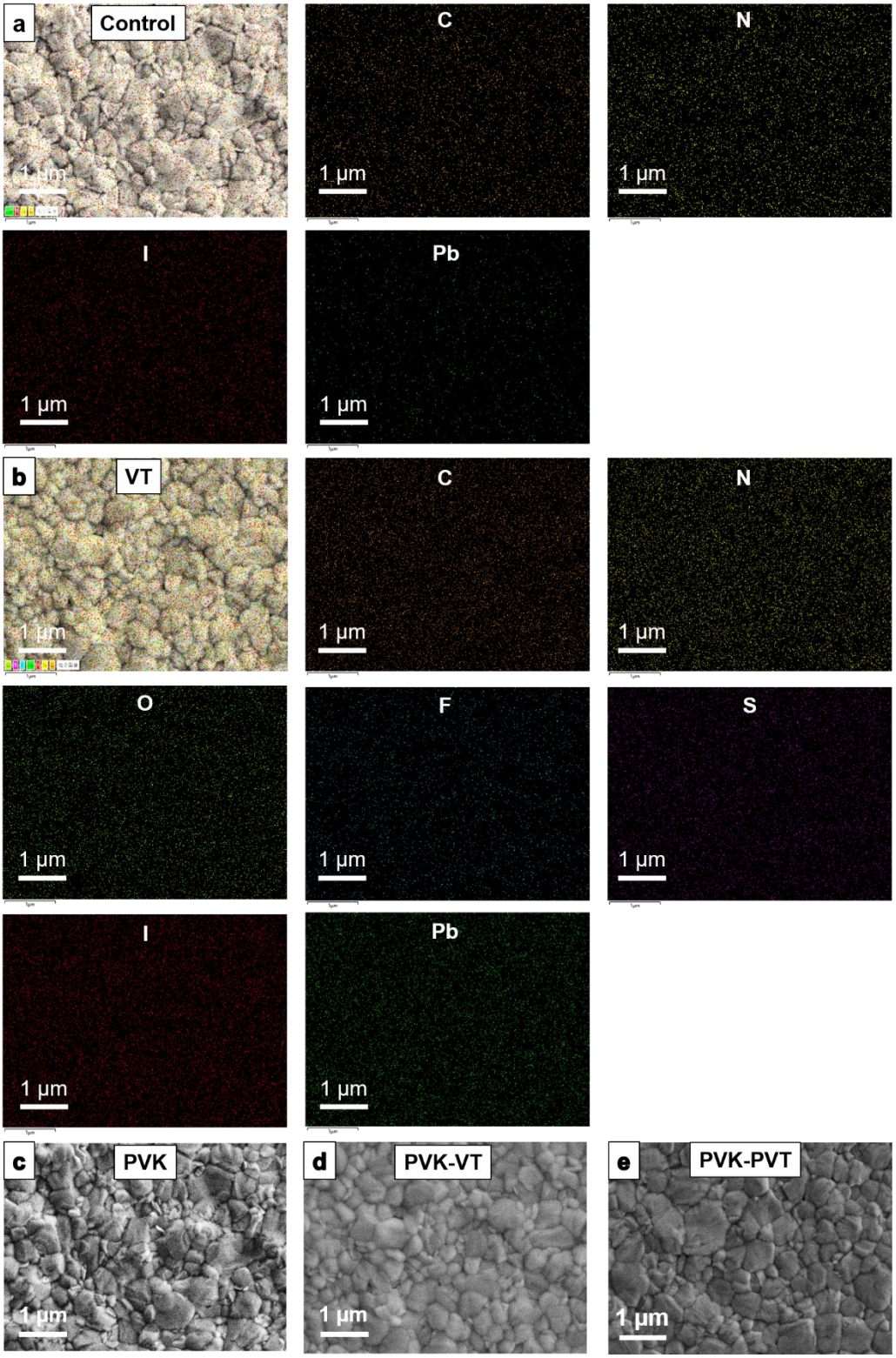

Figure S3. EDS mappings of (a) PVK and (b) PVK-VT films.

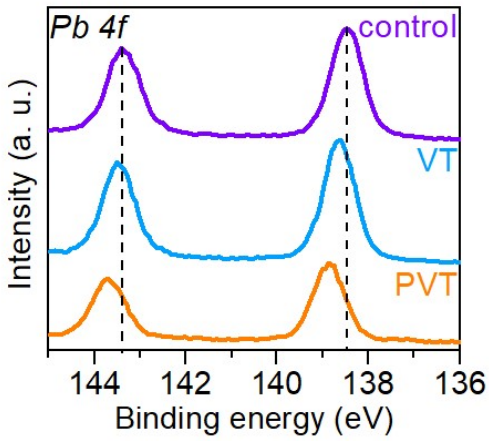

Figure S4. High-resolution XPS Pb 4f spectra of the control, PVK-VT and PVK-PVT films.

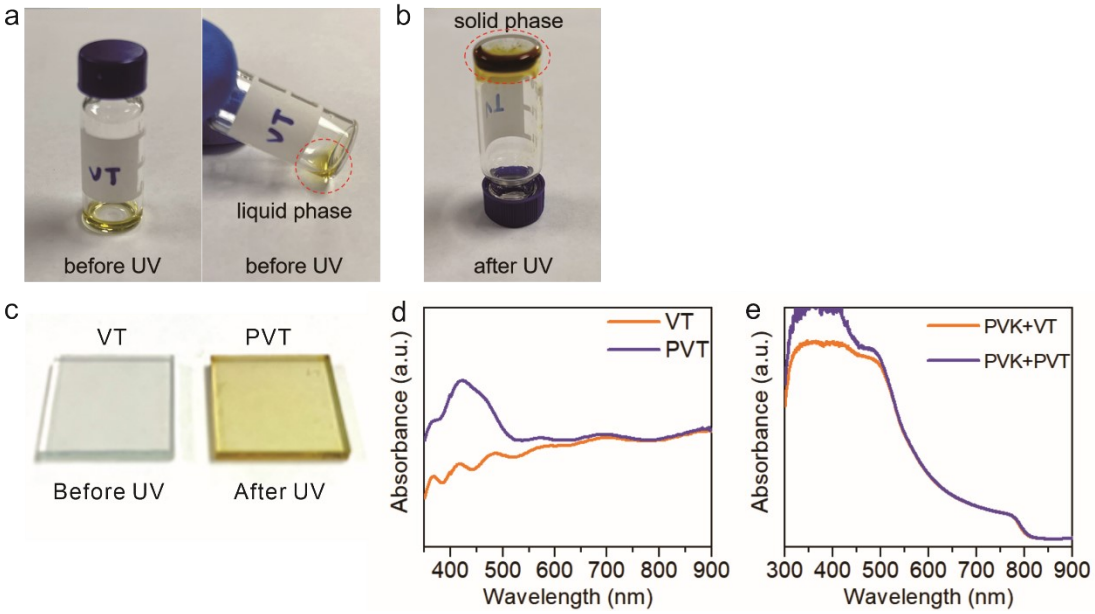

Figure S5. Evidence of VT polymerization. An IPA clear solution of VT (50 mg VT in 50 μL IPA) (a) before and (b) after 3-min UV-exposure; a brown yellow gel was formed, consistent with one previous report (*Nat. Commun.* **2018**, 9, 3806). (c) Photographs and (d) UV-vis spectra of VT film on FTO before and after 3-min UV-exposure; 2 mg/mL VT solution in IPA was used here. (e) UV-vis spectra of PVK-VT film before and after 3-min UV-exposure; 2 mg/mL VT solution in IPA was also used here. The thick VT layer after polymerization displayed an obvious yellow appearance (S5c), and the UV-vis spectra of polymerized VT layer on both FTO (S5d) and perovskite (S5e) appeared an absorption around 400 nm, demonstrating successful VT

polymerization.

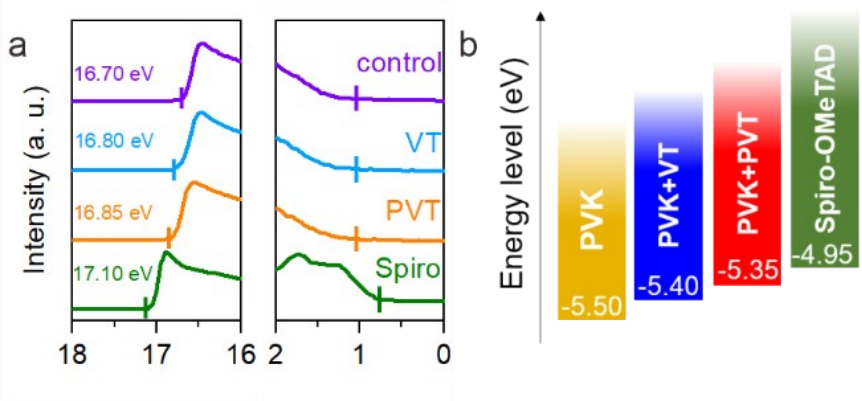

Figure S6. (a) UPS spectra and (b) energy levels of various perovskite-based films. The left panel of Figure 6a shows the secondary electron cutoff regions and its right panel shows the magnified spectra near the Fermi edges.

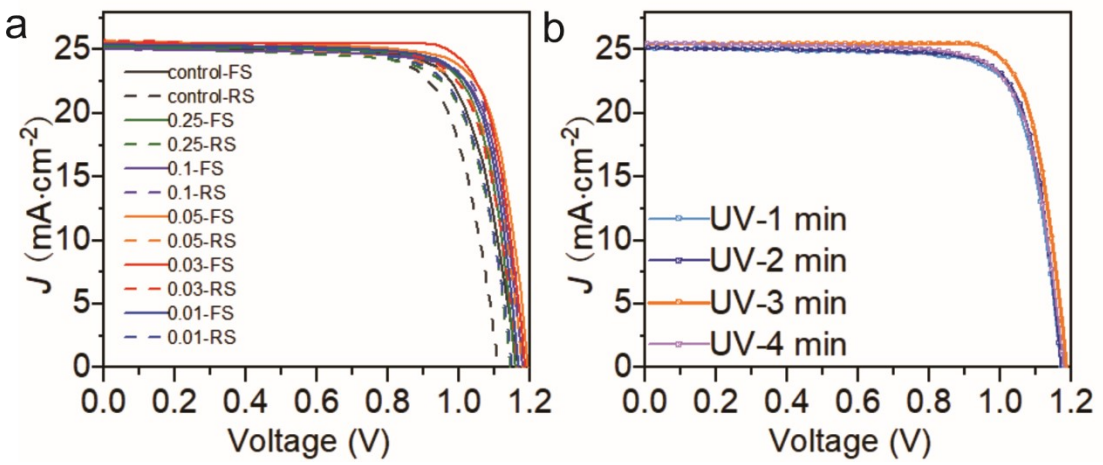

Figure S7. *J-V* curves for PSCs (a) without and with PVT in different concentrations (unit: mg/mL) and (b) different UV-exposure time. The detailed photovoltaic data were shown in Tables S1,2.

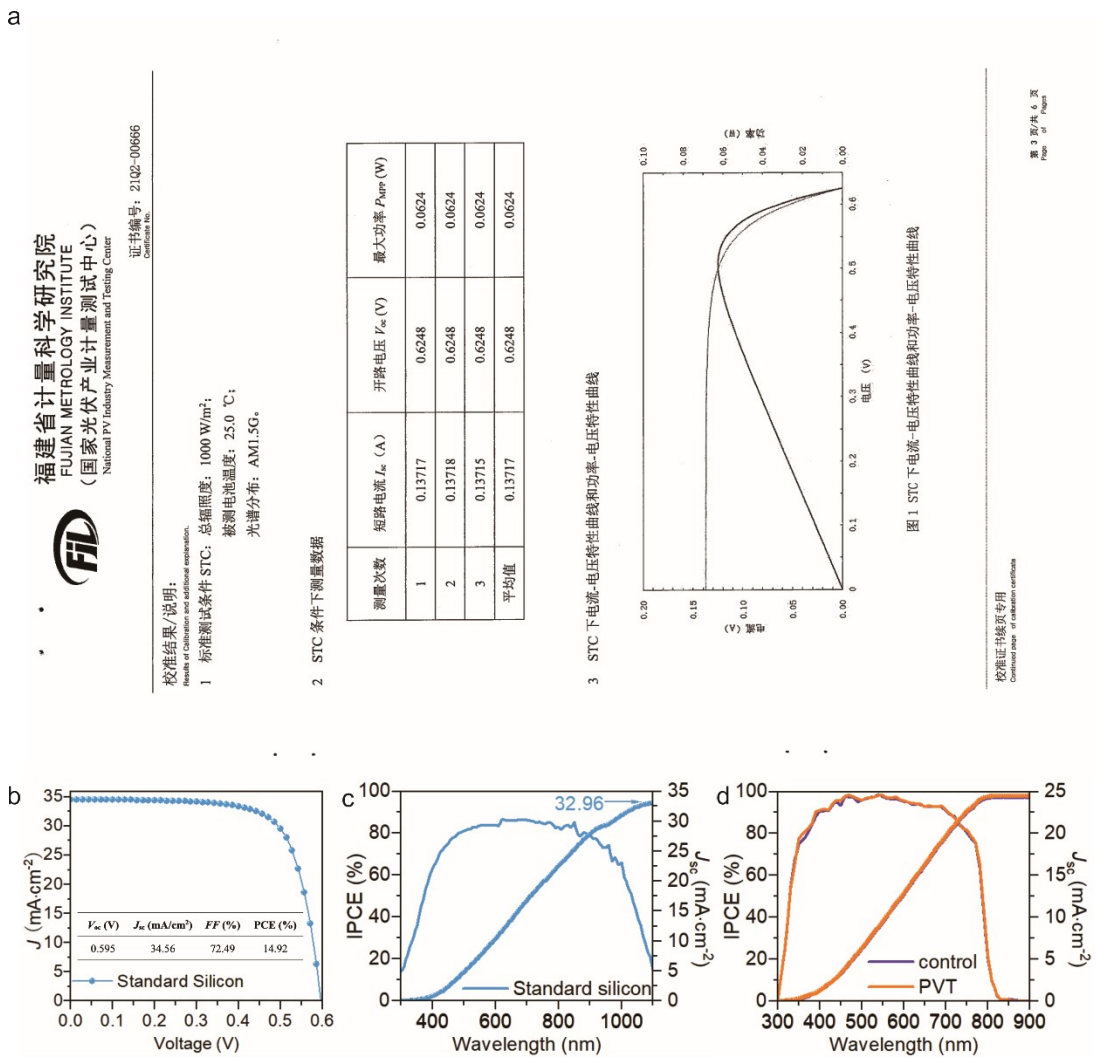

Figure S8. *J-V* curves of a standard silicon solar cell (4 cm^2) measured by (a) third-party certification and (b) our lab; IPCE spectra and integrated J_{sc} of (c) the standard silicon solar cell and (d) as-fabricated PSCs. To convince the measured results, a standard silicon solar cell with a third-party certification has been used to calibrate the *J-V* and IPCE devices, until the current densities from our measurement and the third-party certification matched well (with mismatch <5%). Then the *J-V* curves and IPCE spectra of our samples were collected after calibration.

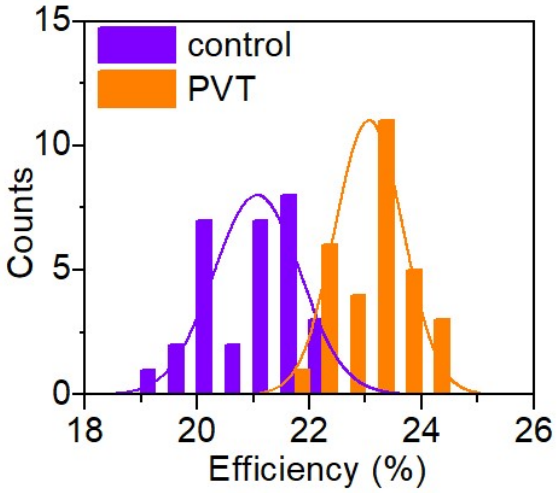

Figure S9. PCE distribution of 30 individual PSCs without or with PVT.

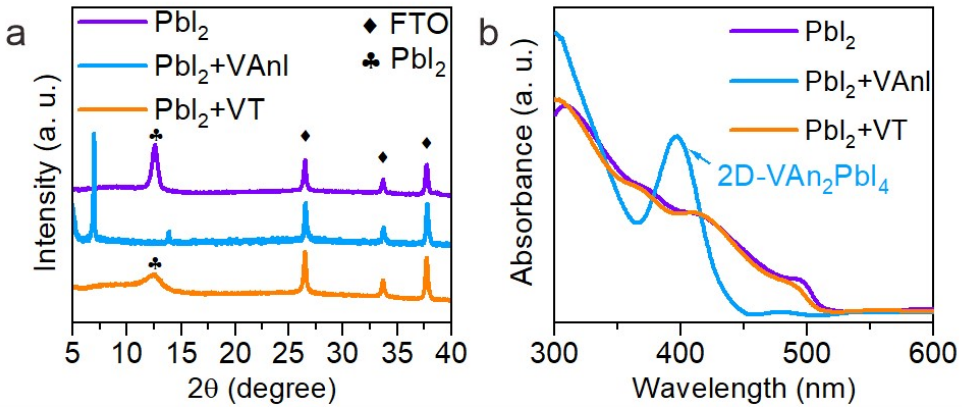

Figure S10. (a) XRD patterns and (b) UV-vis absorption spectra of PbI_2, PbI_2+VAnI and PbI_2+VT films on FTO. VAnI refers to vinylaniline iodine.

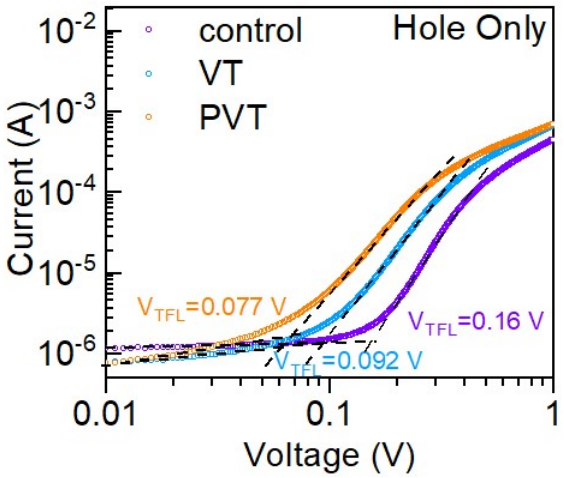

Figure S11. SCLC measurement of small-area devices with the basic structure of FTO/NiO_X/perovskite/P3HT/Au.

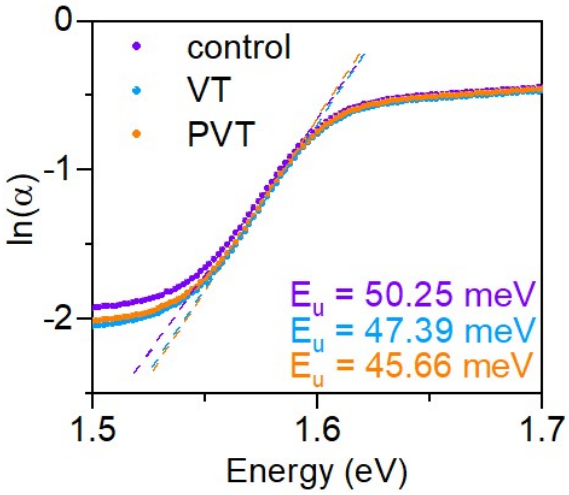

Figure S12. Urbach energy of perovskite-based films calculated by $\alpha = \alpha_0 \exp(h\upsilon/E_u)$, where α is the absorption coefficient of various films and hυ is the photon energy.

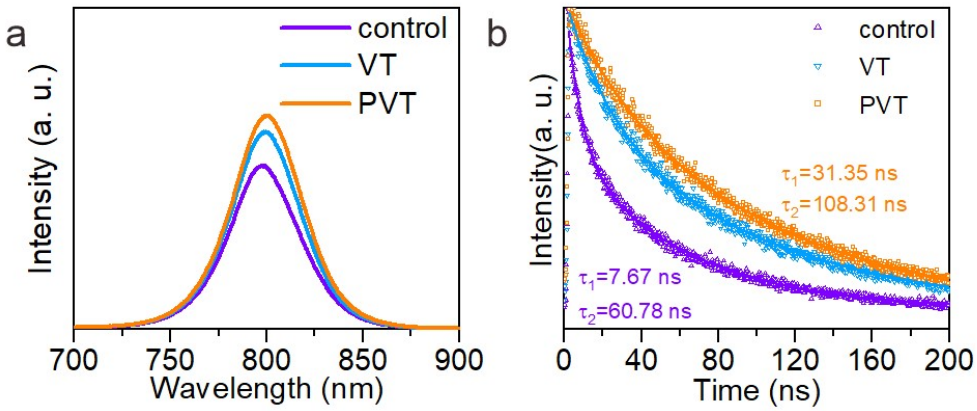

Figure S13. (a) PL and (b) TRPL spectra of perovskite-based films.

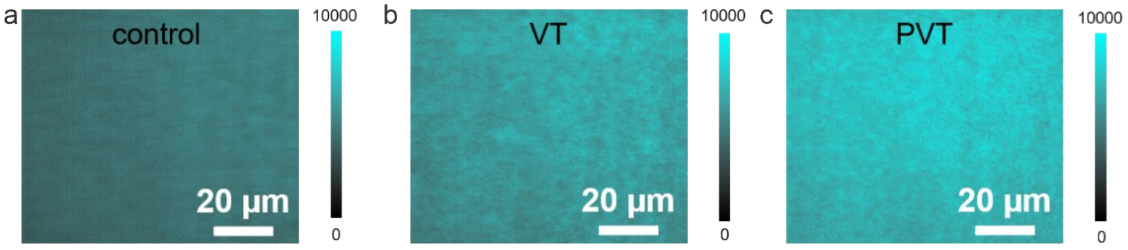

Figure S14. PL mapping of (a) the control, (b) PVK-VT and (c) PVK-PVT films under an excitation wavelength of 532 nm.

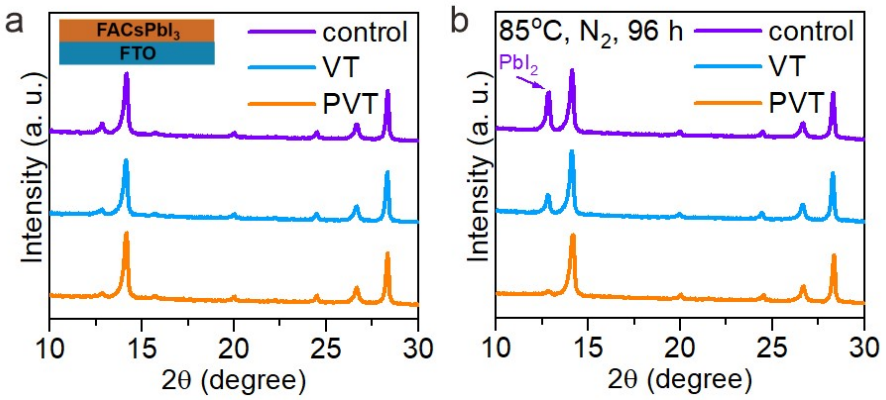

Figure S15. XRD patterns for perovskite-based films stored in N_2 at 85°C for (a) 0 h (b) 96 h.

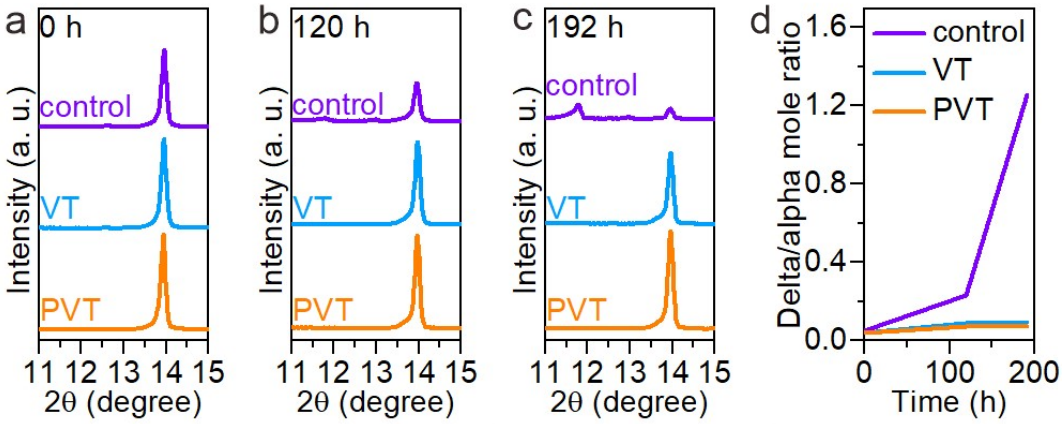

Figure S16. (a-c) XRD patterns of perovskite-based films stored in air for different aging time (room temperature and 60-70% RH). (d) Evolution of relative molar ratios of δ-$FAPbI_3$/α-$FAPbI_3$. The relative ratios were extracted from Figure S16a-c.

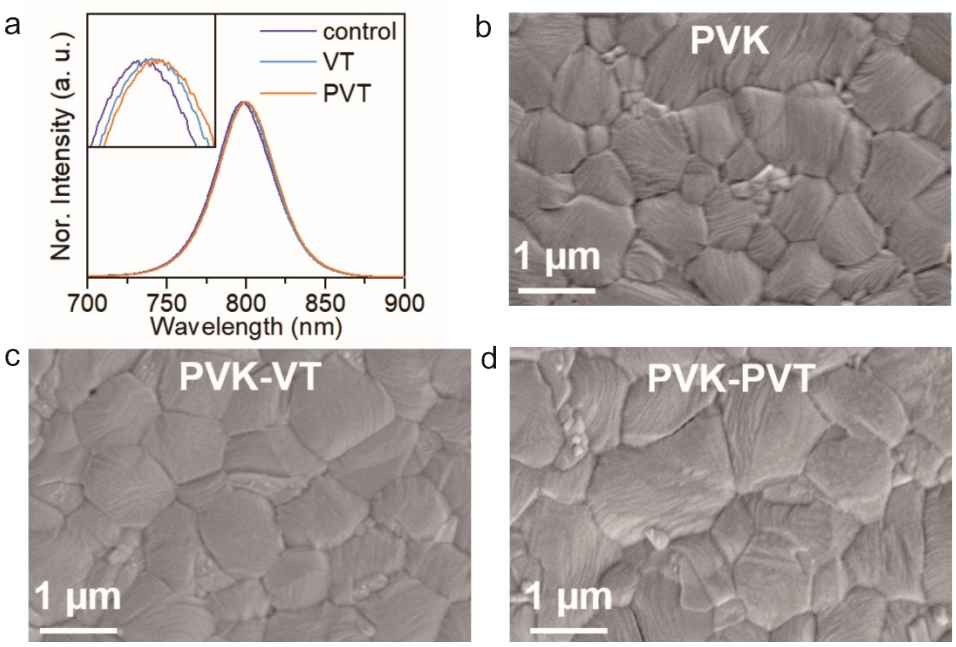

Figure S17. (a) PL emission spectra of the control, PVK-VT and PVK-PVT films. Top-view SEM image of b) PVK, c) PVK-VT and d) PVK-PVT films. The polymerization-induced lattice shrinkage was indicated by the shift of PL positions and change of surface morphologies.

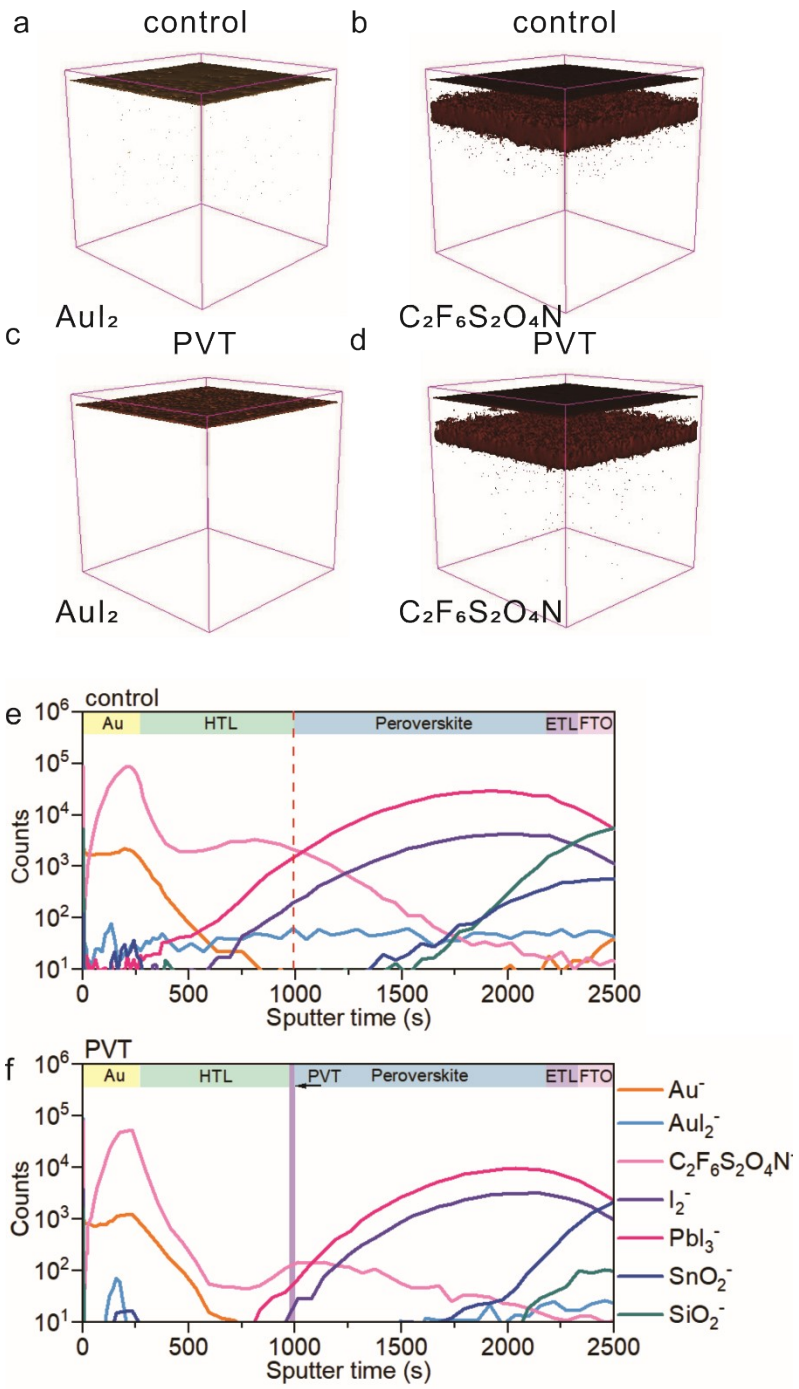

Figure S18. ToF-SIMS 3D depth profiles of PSCs in terms of (a,c) AuI_2^- and (b,d) $C_2F_6S_2O_4N^-$ ions. Note that the $C_2F_6S_2O_4N^-$ signals came from Spiro-OMeTAD with Li-TFSI additive. ToF-SIMS 1D depth profiles of PSCs (e) without or (f) with PVT interlayer between perovskite and HTL. Above data were collected in negative ion mode. The results demonstrate that the PVT layer functioned as barrier layer at the interface between perovskite and HTL to block I migration upward Au and Li-TFSI downward perovskite layer.

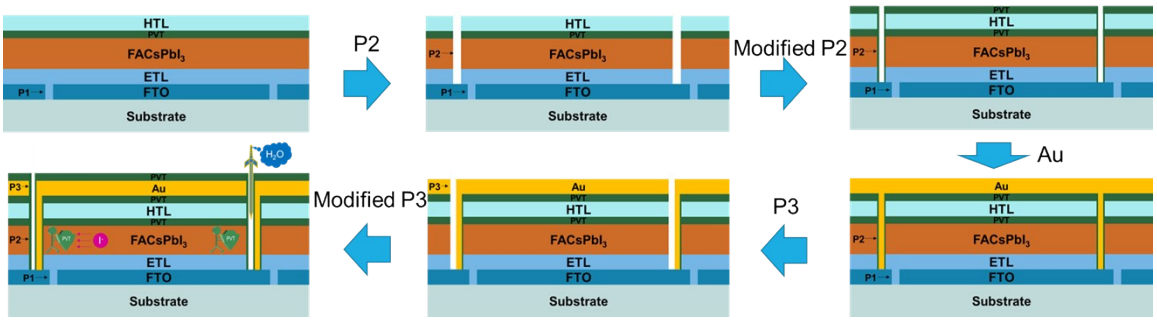

Figure S19. Schematic illustration of our modified laser-scribing (P2 and P3) processes for high-stability multi-interfacial PSMs.

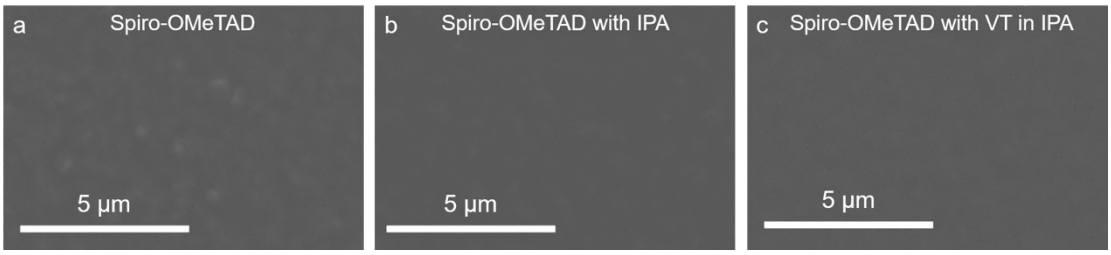

Figure S20. SEM images of FTO/PVK-PVT/Spiro-OMeTAD films (a) before treatment and after (b) IPA or (c) VT/IPA treatment. The treated FTO/PVK-PVT /Spiro-OMeTAD films maintained their original morphologies and no exposure of perovskite films was found, indicating no destroy of underlaying HTL.

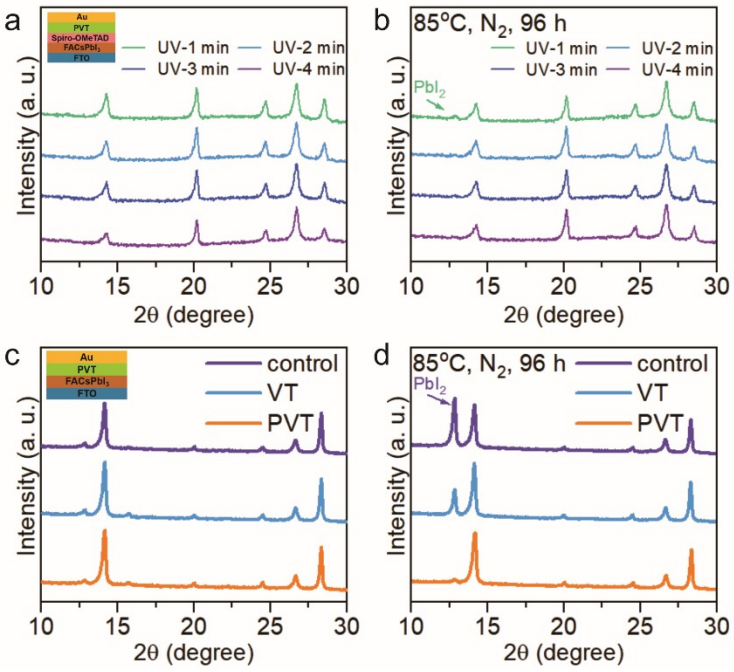

Figure S21. Effects of PVT at different interfaces: (a,b) between HTL and Au, (c,d)

between perovskite and Au. (a,b) XRD patterns for FTO/PVK/HTL/Au devices stored in N_2 at 85°C for (a) 0 h (b) 96 h. The devices were modified with PVT at the interface between HTL and Au, and the PVT was obtained with different UV-exposure time. It was found that the optimized time of UV-exposure was 3 min. (c,d) XRD patterns for FTO/PVK/Au devices stored in N_2 at 85°C for (c) 0 h (d) 96 h. It was found that the perovskite-Au interface was stabilized after PVT modification.

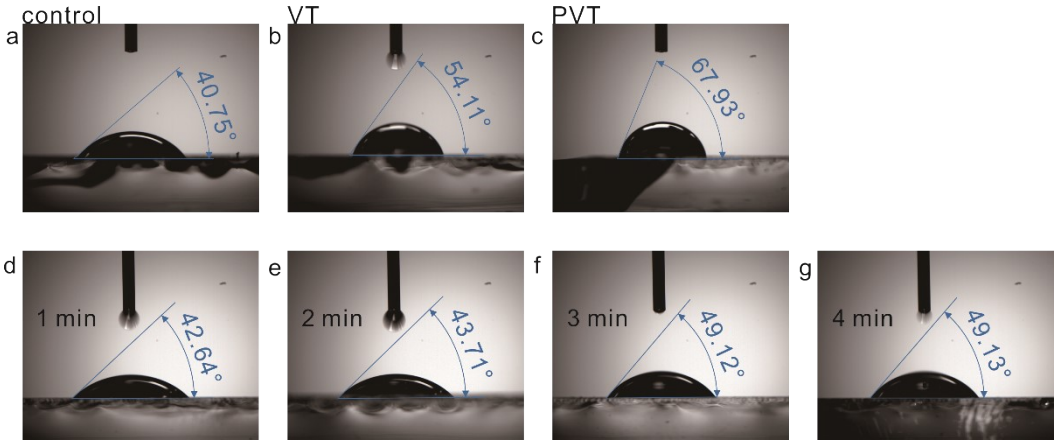

Figure S22. Water contact angles of different substrates: (a-c) perovskite-based films, (d-g) PVK-PVT-HTL/Au film with different UV-exposure time to form PVT on Au.

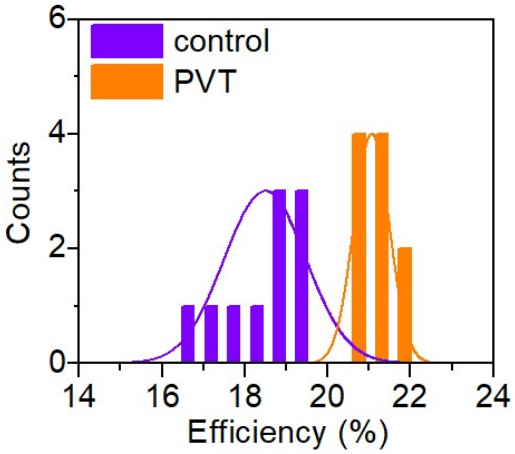

Figure S23. PCE distribution of 10 individual PSMs without or with PVT. The as-fabricated PSMs with and without PVT modification exhibited average efficiency of 21.07±0.41% and 18.50±0.82%, respectively.

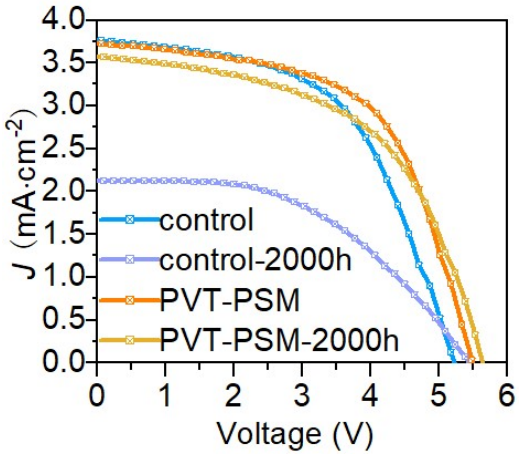

Figure S24. *J-V* curves of PSMs (6 × 6 cm^2) before and after 85°C/85% RH aging. The NiPc was used as hole transfer layer for aging measurements.

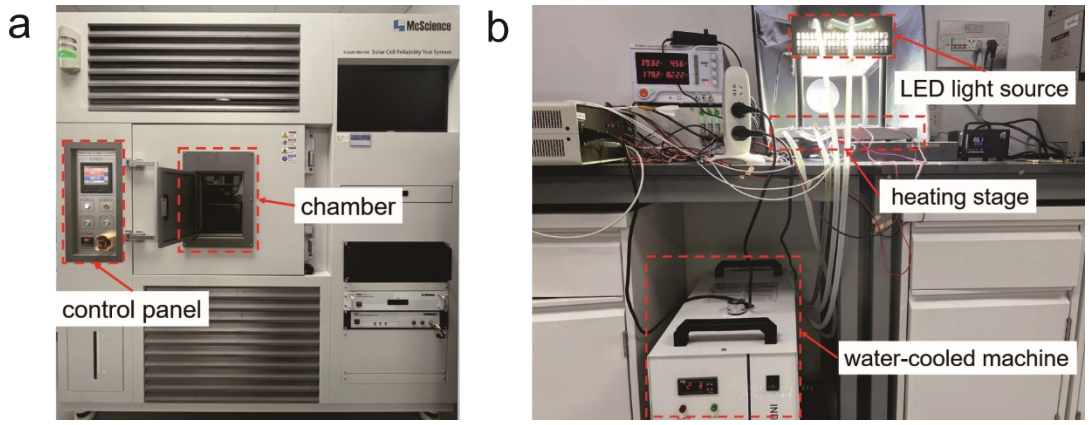

Figure S25. Pictures of aging devices for tests under the condition of (a) 85°C/85% RH or (b) 85°C+one-sun. For 85°C/85% RH test, a solar cell reliability test system (McScience, K3600 MH100) was used. For 85°C aging temperature during illumination tracking, the underlaying heating plate (on which the tested PSMs were put) maintained 85°C without fluctuation, and a circulating cooling system was used for the LEDs of one-sun illumination.

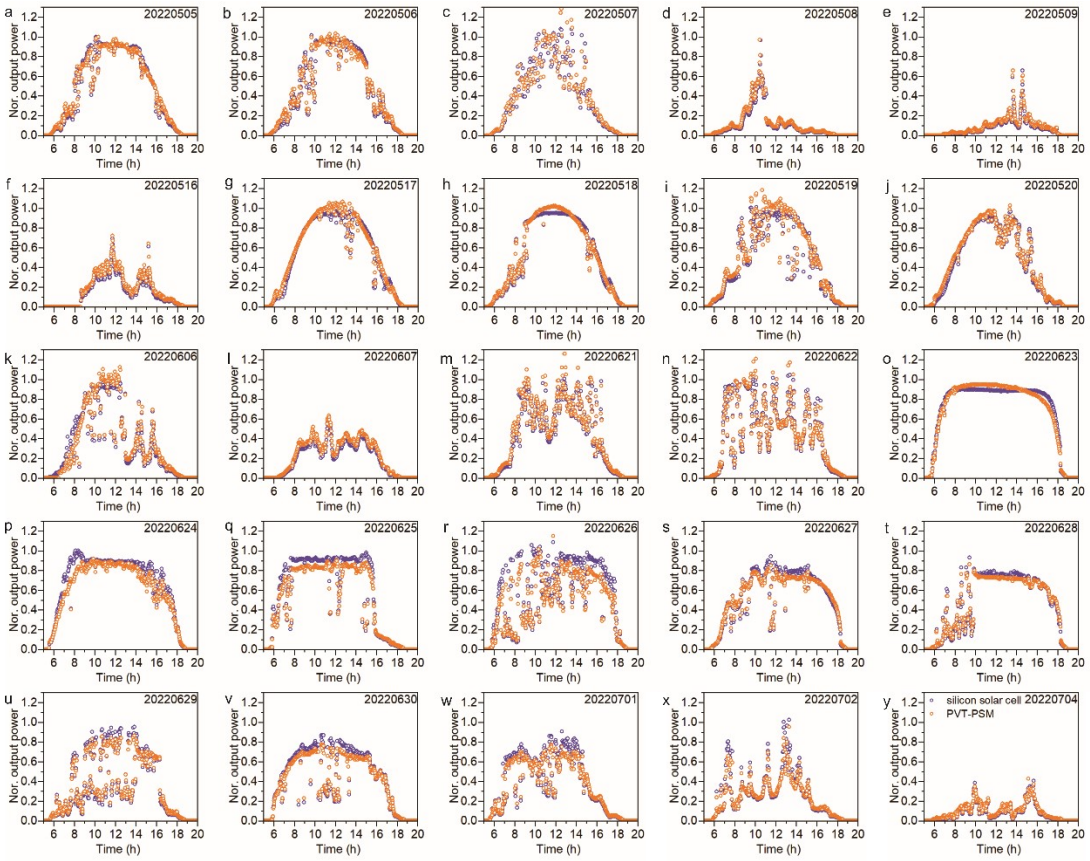

Figure S26. Variation of output powers of one PVT-PSM and one silicon solar cell, normalized to the maximum data of the first day (20220505) for comparison. The intensity of natural light was also collected real time on the "Light intensity detector" as shown in the outdoor photovoltaics-to-energy-storage system (Figure 5a). The system was put outdoors in the Xiang'an campus of Xiamen University (24.4°N, 118.2°E). In order to maximize the use of solar energy, the module with automatic light-seeking function was introduced into outdoor photovoltaics-to-energy storage on June 21, 2022. Note that figures from a to l correspond to outdoor photovoltaics-to-energy storage without automatic light-seeking function, and Figures from m to y correspond to outdoor photovoltaics-to-energy storage with automatic light-seeking function. The experimental date was shown in the insert, and the corresponding weather can be found here:

https://www.timeanddate.com/weather/china/xiamen/historic?month=5&year=2022

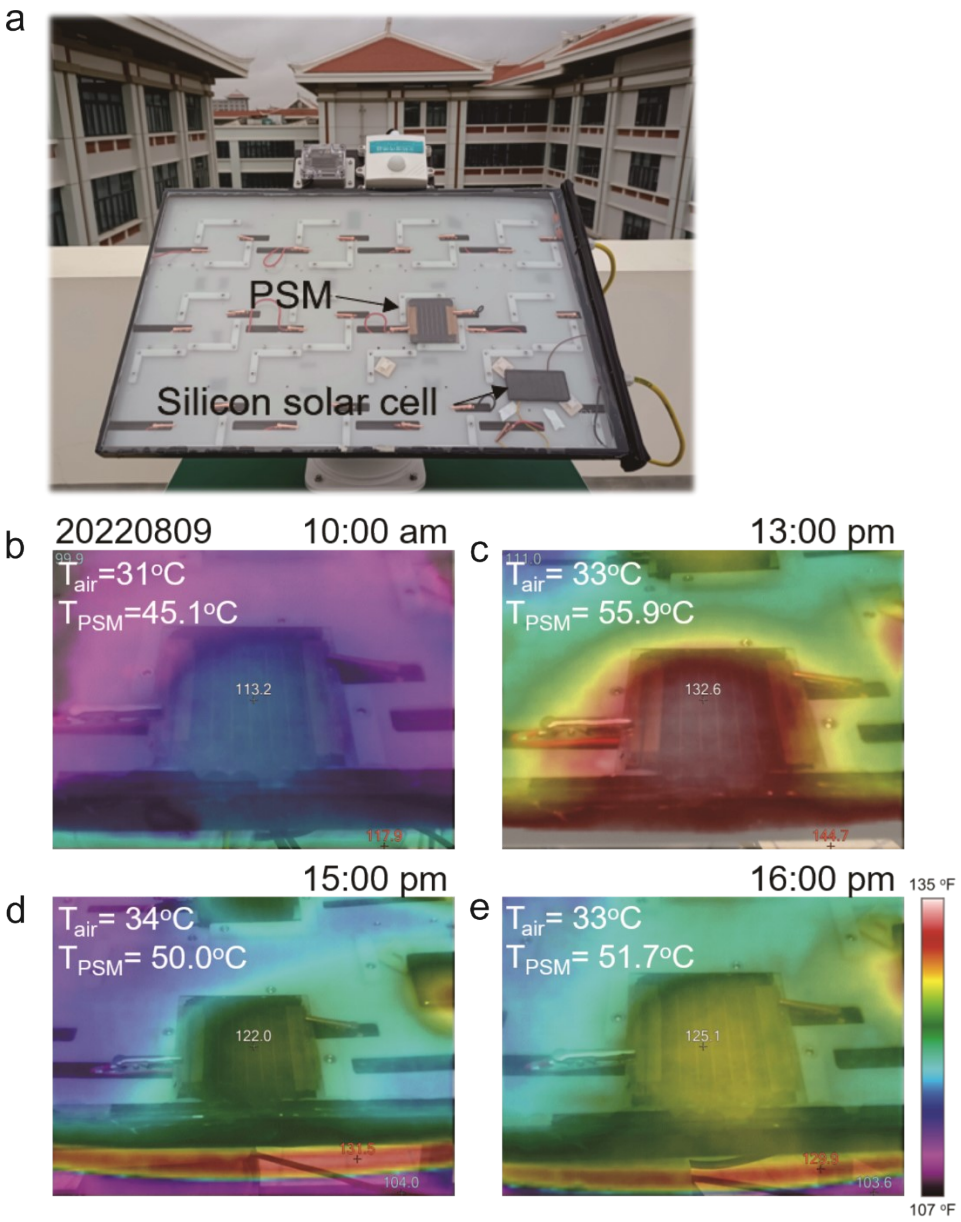

Figure S27. (a) Photograph of our home-made outdoor photovoltaics-to-energy-storage system with automatic light-seeking function. (b-e) Surface temperature evolution of one PVT-PSM working under Sun, monitored by infrared thermal imaging. (T_{air} = ambient air temperature, T_{PSM}=PSM surface temperature)

Table S1. Photovoltaic performances for PSCs without and with PVT in different concentrations.

Entry	V_{oc} (V)	J_{sc} (mA/cm^2)	*FF* (%)	PCE (%)
control-RS	1.168	25.20	75.21	22.14
control-FS	1.111	25.65	72.64	20.70
0.25 mg/mL-RS	1.158	25.20	78.45	22.89
0.25 mg/mL-FS	1.146	25.18	74.48	21.49
0.1 mg/mL-RS	1.178	25.05	78.21	23.07
0.1 mg/mL-FS	1.184	25.03	78.59	23.29
0.05 mg/mL-RS	1.193	25.64	77.84	23.81
0.05 mg/mL-FS	1.178	25.60	74.39	22.44
0.03 mg/mL-RS	1.185	25.47	80.69	24.35
0.03 mg/mL-FS	1.166	25.34	75.08	22.64
0.01 mg/mL-RS	1.166	25.38	78.07	23.11
0.01 mg/mL-FS	1.151	25.45	74.02	21.68

Table S2. Photovoltaic performances for PSCs with PVK-VT after different UV-exposure time.

Entry	V_{oc} (V)	J_{sc} (mA/cm^2)	*FF* (%)	PCE (%)
UV-1 min	1.170	25.11	77.67	22.81
UV-2 min	1.170	25.11	78.83	23.17
UV-3 min	1.185	25.47	80.69	24.35
UV-4 min	1.177	25.49	76.93	23.08

Table S3. Summary of stress-related parameters.

Entry	E	k	Residual Stress (GPa)	Release Residual Stress (%)
control	6.94	0.20	0.47	N/A
VT	4.33	0.12	0.17	62.7%
PVT	5.61	-0.035	-0.065	114.0%

Table S4. Photovoltaic performances of PSMs without or with PVT.

Entry	V_{oc} (V)	J_{sc} (mA/cm^2)	*FF* (%)	PCE (%)
control-6×6 cm^2-RS	8.488	2.97	74.41	18.74
control -6×6 cm^2-FS	8.126	2.99	65.80	16.01
PVT-6×6 cm^2-RS	9.370	3.08	76.17	22.01
PVT-6×6 cm^2-FS	9.037	3.10	69.07	19.35
control-10×10 cm^2-RS	13.364	1.58	70.17	14.83
control-10×10 cm^2-FS	12.621	1.60	54.18	10.94
PVT-10×10 cm^2-RS	15.516	1.79	71.65	19.90
PVT-10×10 cm^2-FS	14.848	1.75	60.60	15.75

Table S5. PCE statistics of 6 × 6 cm^2 PSMs without or with PVT.

Entry	V_{oc} (V)	J_{sc} (mA/cm^2)	*FF* (%)	PCE (%)
Control	7.649	2.97	73.14	16.60
	8.675	2.93	67.57	17.19
	8.640	2.76	73.70	17.60
	8.546	2.86	76.36	18.68
	8.855	2.83	75.53	18.92
	8.898	2.99	71.15	18.95
	8.648	3.01	73.19	19.04
	8.750	2.96	74.46	19.26
	8.727	2.97	74.56	19.34
	8.670	3.04	73.40	19.36
PVT	9.107	3.09	73.51	20.65
	9.009	3.07	74.80	20.71
	9.137	3.04	74.72	20.77
	8.827	2.99	78.82	20.83
	9.153	3.06	74.81	20.96
	9.124	3.07	74.95	20.97
	9.001	3.10	75.45	21.04
	9.133	3.08	75.29	21.15
	9.291	3.02	76.88	21.61
	9.370	3.08	76.17	22.01

Table S6. Photovoltaic performances of PSMs before and after aging at 85°C and 85% RH.

Entry	V_{oc} (V)	J_{sc} (mA/cm^2)	*FF* (%)	PCE (%)
Control-0h	5.218	3.76	54.62	10.72
control-2000h	5.437	2.12	48.87	5.63
PVT-0h	5.489	3.73	58.11	11.88
PVT-2000h	5.641	3.57	53.67	10.82

Table S7. Performance comparison of PSMs.

Device structure	PSMs' PCE (Active area)	Aging condition of PSMs	Maintain initial PCE	References
ITO/ NiO_X/ Perovskite/ DBL/ BCP/ PCBM/ Ag (p-i-n)	15.6% (36.0 cm^2)	85°C / 85% RH (encapsulation)	95% (1000 h)	*Joule*, 2019, **3**, 1-13
ITO/ PTAA/ Perovskite/ C60/ BCP/ Ag (p-i-n)	16.4% (63.7 cm^2)	One-sun (encapsulation)	87% (1000 h)	*Sci. Adv.*, 2019, **5**, eaax7537
FTO/ TiO_2/ SnO_2/ Perovskite/BJ-GO/ TFB/ Cr/ Au (n-i-p)	15.3% (35.8 cm^2)	85°C / 85% RH (encapsulation)	>90% (1000 h)	*Adv. Energy Mater.*, 2021, **11**, 2003301
ITO/ PTAA/ Perovskite / C60/BCP/ Cu (p-i-n)	20.2% (30.0 cm^2)	85°C / 85% RH (encapsulation)	98% (>1000 h)	*Nat. Energy*, 2021, **6**, 633–641
FTO/ SnO_2/ 3D-perovskite/2D-perovskite/ Spiro-OMeTAD/Au (n-i-p)	19.5% (65 cm^2)	N/A	N/A	*Science*, 2021, **372**, 1327–1332
FTO/ QD-SnO_2/ Perovskite/ Spiro-OMeTAD/ Au (n-i-p)	21.7% (20.0 cm^2) 20.6% (64 cm^2)	N/A	N/A	*Science*, 2022, **375**, 302–306
FTO/ c-TiO_2/ m-TiO_2/ Perovskite/ Spiro-OMeTAD/ Au (n-i-p)	22.7% (24.6 cm^2)	N/A	N/A	*Nat. Nanotechnol.*, 2022, **17**, 598–605
FTO/ c-TiO_2/ m-TiO_2/ Perovskite/ NiO_x-P3HT/ Au (n-i-p)	16.8% (18 cm^2)	85°C / 85% RH (encapsulation)	91% (1000 h)	*Adv. Funct. Mater.*, 2022, 2201423
FTO/ SnO_2/ Perovskite/Spiro-OMeTAD/ Au (n-i-p)	20.5% (22.4 cm^2) 15.3% (205 cm^2)	One-sun / N_2/ ~30°C (unencapsulation)	T_{80} (>1000 h)	*Nat. Energy*, 2022, **7**, 528–536
FTO/ $ZnTiO_3$-ZnS/ Perovskite/ PVT/ HTL/ Au (n-i-p)	22.0% (18 cm^2) 19.9% (54 cm^2) (use Spiro-OMeTAD as HTL)	85°C/ 85% RH (use NiPc as HTL; encapsulation)	>97% (1000 h) >91% (2000 h)	This work
		85°C/ 60% RH + one-sun	>90% (300 h)	
		Outdoor & day-night cycling	>95% (25 day)	

References:

1. F. Han, Y. Wu, R. He, et al., *Sol. RRL*, 2021, **5**, 2000654.
2. R. Chen, Y. Wang, S. Nie, et al., *J. Am. Chem. Soc.*, 2021, **143**, 10624-10632.
3. M. D. Segall, P. J. D. Lindan, M. J. Probert, et al., *J. Phys. Condens. Matter*, 2002, **14**, 2717-2744.
4. S. J. Clark, M. D. Segall, C. J. Pickard, et al., *Z. Med. Phys.*, 2005, **220**, 567-570.
5. J. P. Perdew, J. A. Chevary, S. H. Vosko, et al., *Phys. Rev. B. Condens Matter*, 1992, **46**, 6671-6687.
6. C. Zhu, X. Niu, Y. Fu, et al., *Nat. Commun.*, 2019, **10**, 815.
7. H. Wang, C. Zhu, L. Liu, et al., *Adv. Mater.*, 2019, **31**, 1904408.
8. J. Wu, Y. Cui, B. Yu, et al., *Adv. Funct. Mater.*, 2019, **29**, 1905336.